Brain Advance Access published September 19, 2006

doi:10.1093/brain/awl238 *Brain* (2006) Page 1 of 13

Pathological consequences of VCP mutations on human striated muscle

Christian U. Hübbers,[1,*] Christoph S. Clemen,[1,2,*] Kristina Kesper,[3] Annett Böddrich,[7] Andreas Hofmann,[9] Outi Kämäräinen,[9] Karen Tolksdorf,[3] Maria Stumpf,[1] Julia Reichelt,[1] Udo Roth,[2] Sabine Krause,[8] Giles Watts,[10] Virginia Kimonis,[10] Mike P. Wattjes,[4] Jens Reimann,[3] Dietmar R. Thal,[5] Katharina Biermann,[6] Bernd O. Evert,[3] Hanns Lochmüller,[8] Erich E. Wanker,[7] Benedikt G. H. Schoser,[8] Angelika A. Noegel[1,2] and Rolf Schröder[1]

[1]Institute of Biochemistry I, [2]Center for Molecular Medicine Cologne, Medical Faculty, University of Cologne, Cologne, [3]Department of Neurology, [4]Department of Radiology, [5]Institute for Neuropathology, [6]Institute of Pathology, University Hospital Bonn, Bonn, [7]Department of Neuroproteomics, Max Delbrück Center for Molecular Medicine, Berlin, [8]Friedrich-Baur-Institut and Department of Neurology, Ludwig Maximilians University of Munich, München, Germany, [9]Institute of Structural and Molecular Biology, School of Biological Sciences, The University of Edinburgh, Edinburgh, UK and [10]Division of Genetics, Children's Hospital Boston, Harvard Medical School, Boston, MA, USA

Correspondence to: Rolf Schröder, MD, Institute of Biochemistry I, Medical Faculty, University of Cologne, Joseph Stelzmann Strauss 52, 50931 Cologne, Germany
E-mail: rolf.schroeder@uni-koeln.de
*These authors have contributed equally to this work.

Mutations in the valosin-containing protein (VCP, p97) gene on chromosome 9p13–p12 cause a late-onset form of autosomal dominant inclusion body myopathy associated with Paget disease of the bone and frontotemporal dementia (IBMPFD). We report on the pathological consequences of three heterozygous VCP (R93C, R155H, R155C) mutations on human striated muscle. IBMPFD skeletal muscle pathology is characterized by degenerative changes and filamentous VCP- and ubiquitin-positive cytoplasmic and nuclear protein aggregates. Furthermore, this is the first report demonstrating that mutant VCP leads to a novel form of dilatative cardiomyopathy with inclusion bodies. In contrast to post-mitotic striated muscle cells and neurons of IBMPFD patients, evidence of protein aggregate pathology was not detected in primary IBMPFD myoblasts or in transient and stable transfected cells using wild-type-VCP and R93C-, R155H-, R155C-VCP mutants. Glutathione *S*-transferase pull-down experiments showed that all three VCP mutations do not affect the binding to Ufd1, Npl4 and ataxin-3. Structural analysis demonstrated that R93 and R155 are both surface-accessible residues located in the centre of cavities that may enable ligand-binding. Mutations at R93 and R155 are predicted to induce changes in the tertiary structure of the VCP protein. The search for putative ligands to the R93 and R155 cavities resulted in the identification of cyclic sugar compounds with high binding scores. The latter findings provide a novel link to VCP carbohydrate interactions in the complex pathology of IBMPFD.

Keywords: VCP; p97; myopathy; cardiomyopathy; IBMPFD

Abbreviations: GST = glutathione S-transferase; IBMPFD = inclusion body myopathy associated with Paget disease of the bone and frontotemporal dementia; PBS = phosphate-buffered saline; SDS = sodium dodecyl sulphate; VCP = valosin-containing protein

Received May 10, 2006. Revised July 26, 2006. Accepted August 8, 2006

Introduction

Autosomal dominant inclusion body myopathy (IBM) associated with Paget disease of the bone (PDB) and frontotemporal dementia (FTD), or IBMPFD (OMIM 605382), is a late-onset multisystem disorder caused by mutations of the valosin-containing protein (VCP) on chromosome 9p13–p12 (Watts *et al.*, 2004; Haubenberger *et al.*, 2005; Schröder *et al.*, 2005). VCP (p97), an ubiquitously expressed member of the AAA-ATPase family, has a tripartite structure comprising an N-terminal domain (CDC48) involved in ubiquitin binding, and two central

D1- and D2-domains that bind and hydrolyse ATP (DeLaBarre and Brünger, 2003). VCP assembles into functional hexamers with a central cylinder formed by the D-domains surrounded by the N-domains. Apart from R191Q and A232E mutations, which reside in the N-D1-linker region and D1-domain, respectively, all other pathogenic mutations described so far are located in exons coding for the CDC48 domain of the VCP protein (Watts *et al.*, 2004; Haubenberger *et al.*, 2005; Schröder *et al.*, 2005).

VCP has been associated with a wide variety of essential cellular processes comprising nuclear envelope reconstruction, the cell cycle, post-mitotic Golgi reassembly, suppression of apoptosis, DNA damage response and the ubiquitin proteasome protein degradation system (Kondo *et al.*, 1997; Rabouille *et al.*, 1998; Meyer *et al.*, 2000; Hetzer *et al.*, 2001; Rabinovich *et al.*, 2002). Furthermore, VCP along with its co-factors Udf1 and Npl4 as well as Derlin-1 have been implicated to play a central role in endoplasmic reticulum associated protein degradation (ERAD), a process that removes improperly folded proteins from the ER for further degradation by the 26S proteasome (Ye *et al.*, 2001; Rabinovich *et al.*, 2002; Ye *et al.*, 2004; Lilley and Ploegh, 2005).

A further pathogenic link of VCP to protein degradation pathways is highlighted by the observation that VCP-positive protein aggregates have been documented in skeletal muscle and in neurons of the central nervous system of IBMPFD patients (Watt *et al.*, 2004; Schröder *et al.*, 2005). In neurons, these VCP-positive inclusions are exclusively present in the nucleus, whereas in skeletal muscle only cytoplasmic VCP-positive aggregates have been reported. However, VCP-positive aggregates are not specific for IBMPFD and have been documented in a wide variety of neurodegenerative disorders comprising Parkinson's disease, Lewy body disease, Huntington's disease, amyotrophic lateral sclerosis and spinocerebellar ataxia type III (SCAIII; Machado–Joseph disease) (Hirabayashi *et al.*, 2001; Mizuno *et al.*, 2003; Nan *et al.*, 2005). VCP directly interacts with ataxin-3, the protein mutated in SCAIII, and recent *in vivo* studies using *Drosophila* demonstrated that VCP selectively modulates aggregation and neurotoxicity induced by pathogenic ataxin-3 (Böddrich *et al.*, 2006). In the present study we report on the pathological consequences of VCP mutations on human striated muscle *in vivo* and *in vitro*.

Material and methods

Muscle MRI

Whole-body muscle MRI using a 1.5-T scanner, body coil (Philips Gyroscan Intera, Best, The Netherlands) was performed as described previously (Fischer *et al.*, 2005).

VCP mutation analysis

Isolation of DNA and VCP, desmin and αβ-crystallin mutation analysis were performed as described previously (Vicart *et al.*, 1998; Schröder *et al.*, 2003; Watts *et al.*, 2005).

Histological analysis

Cryostat sections (6 μm) from human skeletal muscle were stained by standard diagnostic techniques. Cardiac autopsy material from Patient II was taken from the left and right ventricular and septal walls at the base, mid-cavity and apical levels, and from the left atrial free wall. Sections of paraffin-embedded material were stained by standard diagnostic techniques.

Antibodies

The following primary antibodies were used: VCP rabbit antiserum (kind gift of Dr Chou-Chi Li, National Cancer Institute at Frederick, MD, USA); monoclonal mouse anti-VCP (Affinity BioReagents, USA); monoclonal anti-VCP (BD Biosciences, USA); monoclonal mouse antibody raised against ubiquitin (Novocastra, UK); rabbit anti-ubiquitin polyclonal antibody (Stressgen, Canada); rabbit anti-ubiquitin polyclonal antibody (DAKO, Denmark); monoclonal mouse anti-poly-ubiquitin, clone FK2 (Stressgen, Canada); mouse monoclonal anti-desmin antibody D33 (DAKO, Denmark); rabbit polyclonal anti-αβ-crystallin antiserum (Chemicon, USA); mouse monoclonal antibody raised against Ufd1 (Transduction Laboratories, USA); mouse monoclonal antibody raised against glutathione *S*-transferase (GST) (Amersham Biosciences, Germany); mouse monoclonal anti-His antibody (Qiagen, Germany); mouse monoclonal anti-FLAG M2 antibody (Stratagene, USA); rabbit polyclonal enterokinase cleavage site (FLAG) antibody (Novus Biologicals, USA); TRITC-Phalloidin (Sigma, Germany); monoclonal mouse antibody specifically recognizing GFP (Noegel *et al.*, 2004). Isotype specific secondary antibodies conjugated with fluoroisothiocyanate (FITC), Cy3 or Texas Red, and Alexa568 were applied according to the recommendations of the manufacturers (Southern Biotechnology Associates, USA; Jackson Immunoresearch Laboratories, USA; Molecular Probes, USA). Alternatively, sections incubated with anti-VCP and anti-ubiquitin antibodies were incubated with biotinylated secondary antibodies and the avidin–biotin complex. Visualization was performed with 3,3-diaminobenzidine or the APAP complex as reagent.

Indirect immunofluorescence and imaging of living cells

Indirect immunofluorescence analysis of human skeletal muscle was performed as described previously (Schröder *et al.*, 2003). Transfected cells were seeded on coverslips, washed with phosphate-buffered saline (PBS) and subsequently fixed either in −20°C methanol for 10 min or in 4% formaldehyde for 20 min followed by treatment with 0.5% Triton X-100 and PBS/glycine 0.15% for 5 min each. All following washing steps were performed 5× for 5 min in PBS/glycine. The following staining procedures were performed as described previously (Schröder *et al.*, 2005). Indirect immunofluorescence analysis as well as examination of living cells was done using a confocal Leica DM-IRBE microscope (Leica, Germany).

Ultrastructural analysis and immunogold electron microscopy

Electron microscopy and desmin immunogold electron microscopy of skeletal muscle were performed as described previously (Schröder *et al.*, 2002).

Gel electrophoresis and western blotting

For one- and two-dimensional gel electrophoresis, preparation of total protein extracts, sodium dodecyl sulphate–polyacrylamide gel electrophoresis (SDS–PAGE), protein transfer and visualization of proteins were carried out as described previously (Clemen *et al.*, 2005).

VCP-cDNA, site-directed mutagenesis and plasmids

Human wt-VCP cDNA was amplified by PCR, adding restriction sites and a FLAG-tag at the 3′ end. The PCR-product was cloned in pGEMTeasy vector (Promega, Germany). The mutations R93C, R155H and R155C were introduced using the site-directed mutagenesis kit (BD Biosciences, USA). PCR products and the obtained plasmids were confirmed by direct sequencing (Perkin-Elmer Cetus, USA). For transfection, the VCP constructs were cloned into the pEGFP-N1 and pEGFP-C1 vectors (Clontech, USA). For viral transduction the cDNAs were cloned into the pBMN vector (Clemen *et al.*, 1999).

Cell culture, transfection, transduction and cell stress experiments

HEK293 cells (ATCC: CRL-1573) and C2F3 myoblasts (Clemen *et al.*, 1999) were grown as described. Normal and IBMPFD primary human myoblasts were grown in skeletal muscle cell growth medium (Promocell, Germany; C-23060 with supplement mix C-39365 added). For differentiation of C2F3 myoblasts the FCS was exchanged for using 1% horse serum. Transient transfection of HEK293 cells was carried out by electroporation (1×10^6 cells, 5 μg plasmid; 475 μF, 240 V, 4 mm cuvette). Stable HEK293 clones were obtained by selection with 1.2 mg/ml G418. Transient transfection of C2F3 cells using Lipofectamin was done according to the instructions of the manufacturer (Invitrogen, Germany). Viral transduction of C2F3 cells was done according to Clemen *et al.* (1999) and www.stanford.edu/group/nolan.

MG132 (Calbiochem, USA; 10 mM stock in DMSO; 5 μM final concentration, 16 h; Kitami *et al.*, 2006; Weihl *et al.*, 2006), *clasto*-lactacystin β-lactone (Calbiochem; 10 mM stock in DMSO; 10 μM final concentration, 24 h; Steinhilb and Gaut, 2001; Waelter *et al.*, 2001), wortmannin (Calbiochem, datasheet 681675; 1 mM stock in DMSO; 1 μM final concentration, 22 h), H_2O_2 (Sigma, Germany; 400 μM final concentration, 16 h; Ardley *et al.*, 2003) were added to normal culturing medium. For osmotic shock experiments, cells were incubated in 150 mM urea dissolved in normal culturing medium (Sigma, Germany; D'Alessandro *et al.*, 2002) for 5 min. The solution was changed to fresh medium and cells were subsequently fixed after 4 min. UV-B irradiation experiments were performed using opened culture dishes containing a minimal volume of PBS in a UV-cross-linker (Hoefer UVC 500, Amersham Pharmacia Biotech, Germany; Westfall *et al.*, 2005) with a total dose of 100 J/m^2 at a wavelength of 254 nm. Cells were further incubated in fresh medium and analysed after 12 h. Mitomycin C treatment (Medac, Germany; 10 μg/ml final concentration; standard protocol) was done for 3 h in normal culturing medium followed by two washing steps with PBS. Cells were subsequently analysed after 1, 7 and 14 days.

Protein-binding studies

GST-, MBP- and His-tagged fusion proteins were expressed in *Escherichia coli* and purified on affinity columns as described previously (Scherzinger *et al.*, 1997) and according to manufacturer's instructions (NEB, USA; Qiagen, Germany). The plasmids pGEX-6P-VCP wt, pGEX-6P-VCP R155H, pGEX-6P-VCP R155C and pGEX-6P-VCP R93C were generated by amplifying the VCP cDNA-fragments from pGEMTeasy vector (*see* above) and subcloning in pGEX-6P-1 (Amersham Biosciences, Freiburg, Germany). The cDNA encoding Ufd1 was obtained from the RZPD (Deutsches Ressourcenzentrum für Genomforschung GmbH, Germany), amplified and cloned into pMAL-c2X (NEB). To produce a His-tagged Npl4 fusion protein, the Npl4 cDNA (kindly provided by H. Meyer, ETH Zürich, Switzerland) was amplified and cloned into pQE30N, a derivative of pQE30 (Qiagen, Germany). The cloning of the ataxin-3 cDNA into pQE has been described (Tait *et al.*, 1998). For *in vitro* binding experiments, GST fusion proteins were bound to glutathione agarose beads and incubated with 0.1 μM MBP-Ufd1, 0.1 μM His-Npl4, 0.1 μM His-ataxin-3 Q22 or combinations of 0.1 μM MBP-Ufd1/His-Npl4 and 0.1 μM MBP-Ufd1/His-Npl4/4 μg tetra-ubiquitin (Biomol, UK) in IP-buffer (50 mM HEPES pH 7.4, 150 mM NaCl, 1.5 mM $MgCl_2$, 1 mM EGTA, 20 mM NaF, 10% glycerol, 1% NP-40 and protease inhibitors) at 4°C for 1 h. After washing the beads four times with IP-buffer, bound proteins were eluted with SDS-sample buffer, boiled for 5 min and analysed by immunoblotting.

Modelling of human valosin-containing protein

The crystal structure of the ND1-domains of mouse VCP in complex with rat p47 has previously been solved at a resolution of 2.9 Å (PDB entry 1s3s; Dreveny *et al.*, 2004).

Since mouse and human VCP protein share 99.5% identity with Ile206 being Val in the mouse protein, we have taken the model from 1s3s and introduced the mutation V206I using the program O (Jones *et al.*, 1991) followed by local refinement. Mutations of interest for this study (R155C, R155H, R93C) were introduced in the same manner. The overall geometry of the models was scrutinized with PROCHECK (Laskowski *et al.*, 1993).

Virtual screening of ligand databases

Two potential ligand-binding pockets were identified from the homology model of ND1-VCP and the automated docking programme LIDAEUS (Wu *et al.*, 2003) was used to screen all structures of a small-molecule database (Sigma catalogue) against the potential ligand-binding pockets. First, a dummy ligand (ADP) was docked in the potential pockets by FlexX (Rarey *et al.*, 1996) to obtain template coordinates for the generation of binding pocket site points with certain characteristic features (electrostatic potential, hydrogen donor, hydrogen acceptor, etc). On the basis of chemical and shape complementation, LIDAEUS finds ligands that complement the features of the binding pocket and generates multiple ligand-binding conformations. The programme then tries to find the best fit of the different poses by ranking the conformations according to various energy scores including hydrophobic interactions, van der Waals and H-bonding. The small-molecule database was prepared for LIDAEUS using the software EDULISS (Wu *et al.*, 2003). As a control, the dummy ligand ADP used for site point generation was also included in the screen. The resulting ligands and poses were analysed with the

graphics programme WITNOTP (A. Widmer, Novartis, Switzerland). A selection of ligands that were docked well inside the pocket was subjected to further analysis including scoring and ligand-protein contacts using the programme LIGPLOT (Wallace *et al.*, 1995).

Results

Clinical phenotype

Patient I: A 74-year-old male patient was regularly seen since age 55. He has a >20-year history of slowly progressive distal muscle weakness predominantly affecting the lower extremities. Signs of progressive cognitive impairment were first noted in his late 60s. Except for Paget's disease in the patient's father, the family history was unremarkable with regard to neuromuscular or psychiatric disorders. Neurological examination in 2005 showed marked generalized weakness and atrophy of distal arms and leg muscles. In addition, axial weakness of the lumbar trunk was noticed. Repeated neuropsychiatric evaluation showed evidence of progressive personality changes and cognitive decline due to frontotemporal brain dysfunction. Axial computed tomography revealed Paget-like bone changes in the right hip. Creatine kinase (CPK) levels had been mildly elevated (115 U/l; normal <80) at the initial examination, but were in the normal range ever since.

Patient II: A 62-year-old female patient was first seen in 1993. At that time, she gave a 3-year history of progressive proximal muscle weakness. Brain MRI performed in 1995 showed frontal and temporal brain atrophy. Her last neurological examination in February 1997 showed a severely demented patient with a flaccid, predominantly proximal tetraparesis. Serum CPK levels were always within normal limits. According to information obtained by her husband in 1998, the mother of the reported patient, her mother's brother as well as one of his children suffered from similar medical conditions. She died of pneumonia and cardiac failure in 1998. Autopsy at that time showed severe generalized wasting of her skeletal muscles, but no signs of Paget's disease of the bone. The total heart weight was 480 g; left ventricular and right ventricular wall thickness was 1.7 and 0.7 cm, respectively. Neuropathological analysis of her brain has been reported previously (Schröder *et al.*, 2005). Neurons exhibited nuclear inclusions containing VCP- and ubiquitin-containing material.

Patient III: A 54-year-old female first presented in May 2003. She gave a 30-year history of slowly progressive muscle weakness and atrophy predominantly affecting her shoulder girdle, trunk and distal leg muscles (Fig. 1A). Her family history was negative for neuropsychiatric, muscular or bone diseases. Paget's disease of the bone confined to the first lumbar vertebra was histologically diagnosed in 2002 (Fig. 1B). She presented no overt neuropsychological or behavioural abnormalities. However, a detailed neuropsychological evaluation in February 2004 revealed a performance far below average (>2 SDs below mean) in the labyrinth task testing for anticipation, and below average (>1 SD below mean) in the figural memory and naming tests, suggesting mild frontotemporal cognitive dysfunction. Brain MRI and cardiological examination gave normal results. Neurological examination showed severe weakness and atrophy of her scapular fixator muscles (deltoid, rhomboid, supra- and infraspinatus) and trunk extensors. In addition, she had slight to moderate muscle weakness of

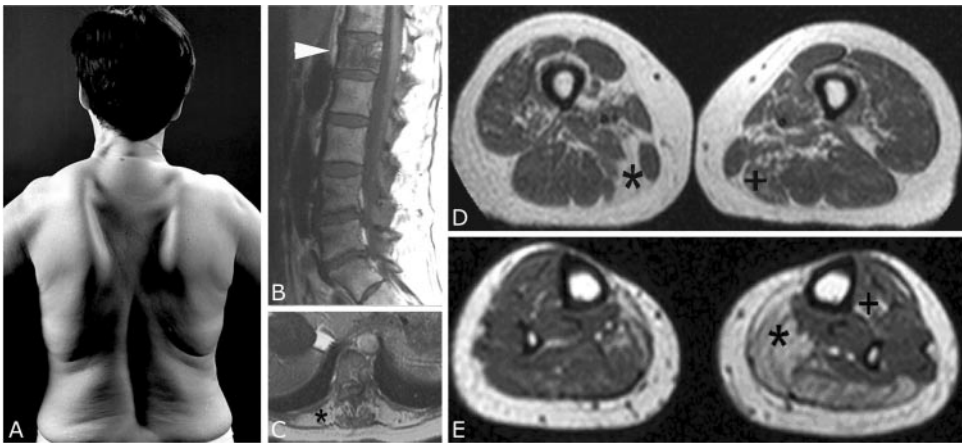

Fig. 1 Clinical and MRI findings in Patient III. (**A**) The marked scapular winging and lumbar lordosis may be noted. (**B**) The sagittal view of the lumbar spine reveals a stripy ossification of the first lumbar vertebra (arrowhead) due to Paget's disease. T_1-weighted TSE-sequence with 600/12 ms (TR/TE), 4 mm slice-thickness. (**C**) The cross-cut view at the level of the thoracic spine demonstrates a complete fatty replacement of the erector spinae muscles (*). T_1-weighted TSE-sequence with 450/17 ms (TR/TE), 5 mm slice-thickness. (**D**) The cross-cut view of the thighs shows a high degree of fatty degeneration of the right semimembranosus muscle (*) and, to a lesser degree, of the left semimembranosus muscle (+). T_1-weighted TSE-sequence with 450/17 ms (TR/TE), 5 mm slice-thickness. (**E**) MRI of the calves depicts marked fatty replacement of the left gastrocnemius muscle (*) as well as signal changes in the anterior compartment muscles (+). T_1-weighted TSE-sequence with 450/17 ms (TR/TE), 5 mm slice-thickness.

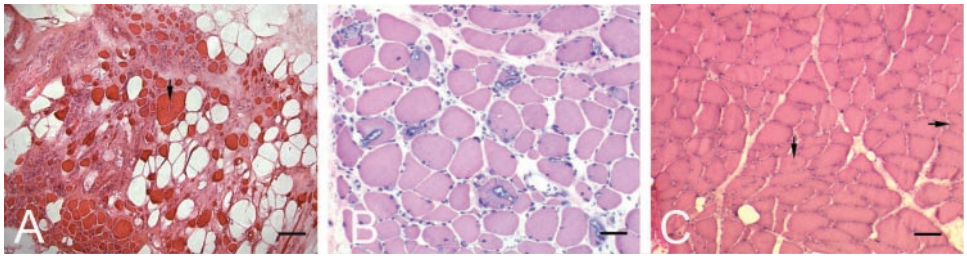

Fig. 2 Morphological analysis of IBMPFD muscle. (**A**) Biopsy from Patient I revealed severe degenerative muscle changes. The marked fatty replacement of muscle fibres, broadening of connective tissue, rounding and atrophy of muscle fibres and hypertrophic fibres may be noted. The arrow denotes a hypertrophic fibre with a central rimmed vacuole. (**B**) Biopsy from Patient II showed the classical picture of an IBM with an abundance of rimmed vacuoles. (**C**) Biopsy from Patient III showed only mild and unspecific myopathological changes. Fibres containing rimmed vacuoles are marked by arrows. [Haematoxylin and eosin staining; bars: (**A**) 100 μm, (**B**) 50 μm, (**C**) 60 μm].

her finger extensor, hip flexor and distal leg muscles. Repeated serum CPK levels were within normal limits. Whole-body MRI demonstrated widespread muscular involvement with pronounced signal changes in her erector spinae, hamstring and calf muscles (Fig. 1C, D and E)

Mutation analysis

Mutation analysis in Patient I revealed a novel heterozygous nucleotide substitution in exon 3 (c.277C → T) of the VCP gene (GenBank AC004472). This mutation is predicted to result in an amino acid substitution from arginine to cystein in codon 93 (R93C) and was not detected in 100 control chromosomes (data not shown). In Patient II, we previously identified a heterozygous mutation in exon 5 leading to an amino acid substitution from arginine to cystein in codon 155 (c.463C → T, R155C; Schröder *et al.*, 2005). Additionally, mutations of the desmin and αβ-crystallin genes were ruled out by direct sequence analysis in this patient. VCP mutation analysis of a DNA sample from Patient III revealed a heterozygous nucleotide substitution causing an amino acid substitution in the same codon from arginine to histidine (c.464G → A, R155H) (data not shown).

Skeletal muscle pathology

Morphological evaluation of a vastus lateralis and tibial anterior biopsy from Patient I showed severe degenerative changes consisting of increased fibre size variation, atrophy of both fibre types, presence of terminal atrophic and angulated fibres, hypertrophic type-1 fibres, degenerating and a few regenerating fibres, 'myopathic grouping' as well as marked fatty replacement of muscle fibres and broadening of connective tissue (Fig. 2A). A diagnostic muscle biopsy taken from the biceps brachii muscle of Patient II displayed the classical myopathological picture of an IBM with an abundance of rimmed vacuoles (Fig. 2B). In contrast, the biopsy from the vastus lateralis muscle in Patient III showed only mild and unspecific myopathological changes consisting of type I fibre predominance, atrophic and hypertrophic fibres (Fig. 2C). In addition, few de- and regenerating fibres could be demonstrated. It is noteworthy that in biopsies from Patient I and III only a few fibres with rimmed vacuoles could be detected. None of the three reported cases showed inflammatory infiltrates.

Double-immunofluorescence analysis of skeletal muscle from Patient III revealed a small number of fibres (<5%) containing cytoplasmic foci of VCP- and ubiquitin-positive protein aggregates (data not shown), whereas the corresponding analysis of the muscle biopsy from Patient II showed a high number of fibres (30–40%) with single or multiple VCP- and ubiquitin-positive cytoplasmic inclusions (Fig. 3A and B). In addition, double-staining with VCP antibody and DAPI (4′,6′-diamidino-2-phenylindole-dihydrochloride) revealed multiple fibres with VCP-positive nuclear inclusions (Fig. 3C and D). Further analysis revealed multiple fibres displaying subsarcolemmal and cytoplasmic areas with increased αβ-crystallin (Fig. 3E) and desmin labelling (Fig. 3F).

A detailed ultrastructural analysis was performed on skeletal muscle from Patient II. The VCP-positive nuclear inclusions consisted of filamentous material (Fig. 4A). In analogy to the abundance of rimmed vacuoles and cytoplasmic VCP and ubiquitin-positive inclusions at the light microscopic level, many fibres contained autophagic vacuoles with haphazardly arranged filamentous material as well as large cytoplasmic areas consisting of densely or loosely packed filamentous material (Fig. 4B). Remarkably, multiple fibres also displayed areas with granulofilamentous material as seen in the group of myofibrillar myopathies (Fig. 4C). Immunogold EM showed a dense desmin-positive labelling of these areas (Fig. 4D).

Cardiac pathology

Post-mortem analysis of the heart of Patient II revealed a marked left ventricular dilatation and thickening of the left ventricular wall (Fig. 5A). Histopathological examination showed cellular hypertrophy of myocytes and in conjunction with multiple small parenchymal scars in both ventricles.

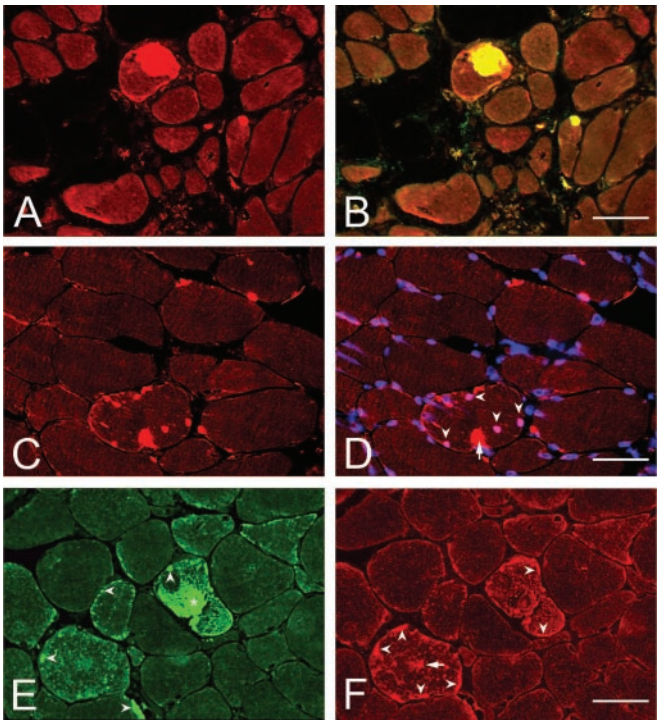

Fig. 3 Indirect immunofluorescence analysis of IBMPFD muscle from Patient II. (**A**) VCP labelling of cytoplasmic aggregates. (**B**) VCP and ubiquitin double-immunofluorescence labelling of cytoplasmic aggregates. (**C**) VCP labelling of cytoplasmic and nuclear aggregates. (**D**) VCP and DAPI labelling. The presence of cytoplasmic (red, arrow) and nuclear (pink, arrowheads) aggregates may be noted. (**E**) Pathological αB-crystallin staining with positive labelling of a giant cytoplasmic (*) and multiple small subsarcolemmal aggregates (arrowheads). (**F**) Pathological desmin staining in two muscle fibres displaying increased subsarcolemmal (arrowheads) and cytoplasmic areas (arrow) with increased desmin immunolabelling. Bars: (**B**) 70 μm, (**D**) 50 μm, (**F**) 40 μm.

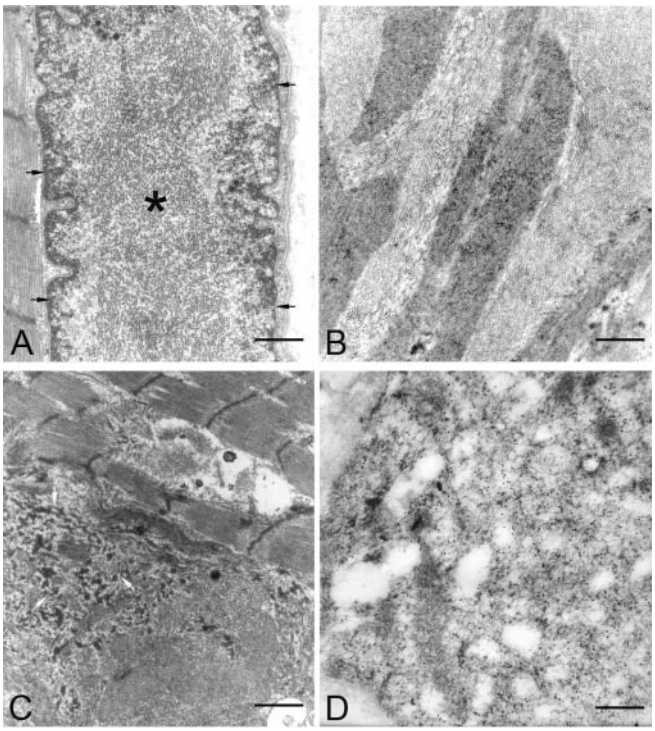

Fig. 4 Ultrastructural analysis of skeletal muscle from Patient II. (**A**) Filamentous nuclear inclusion (*); arrows indicate the nuclear membrane. (**B**) Cytoplasmic area with loosely and densely packed filamentous material. (**C**) The arrows denote an area with granulofilamentous material. (**D**) Immunogold electron microscopy with the monoclonal anti-desmin antibody (mab-D33) and a secondary antibody coupled to 10 nm gold particles showed a dense labelling of filamentous aggregates. Bars: (**A**) 0.5 μm, (**B**) 0.6 μm, (**C**) 0.7 μm, (**D**): 0.25 μm.

Immunostaining of formalin-fixed and paraffin-embedded cardiac tissue revealed multiple cardiomyocytes displaying ubiquitin-positive cytoplasmic and single nuclear inclusions (Fig. 5B and C).

VCP protein expression in IBMPFD muscle

VCP immunoblotting after 1D SDS–PAGE revealed a single band corresponding in size to 97 kDa in all probes analysed without significant changes in the total amount of VCP between normal and R93C-, R155H-, R155C-IBMPFD muscle (Fig. 6). Differential centrifugation of muscle tissue lysates revealed that VCP was exclusively found in the pellet fraction of IBMPFD and normal control muscle (Fig. 6).

VCP immunoblotting after 2D gel electrophoresis of total protein extracts from normal human skeletal muscle revealed a prominent spot at pH 5.20. In addition, a second spot with weaker signal intensity was detected at the position of pH 5.16, which corresponds well with the calculated pI 5.14. A corresponding analysis of diseased skeletal muscle (R155H, R155C) showed an identical pattern compared with control muscle (data not shown).

Analysis of normal and IBMPFD primary human myoblasts

In order to study pathological protein aggregate formation in cultured cells, we analysed normal and IBMPFD (155C VCP mutant) in primary human myoblasts. Immunostaining using FK2 (Fig. 7) and VCP antibodies (data not shown) revealed an identical reticular staining pattern in normal and IBMPFD myoblasts. In contrast to IBMPFD muscle, no pathological protein aggregate formation could be detected.

Wild-type versus mutant VCP in transfected cells

The following transfection and transduction experiments were performed: (i) Wt- and mutant-GFP-VCP-FLAG and VCP-FLAG-GFP were transiently and stably expressed in HEK293 cells; (ii) wt- and mutant-VCP-FLAG-GFP were transiently expressed in C2F3 myoblasts; (iii) wt- and the

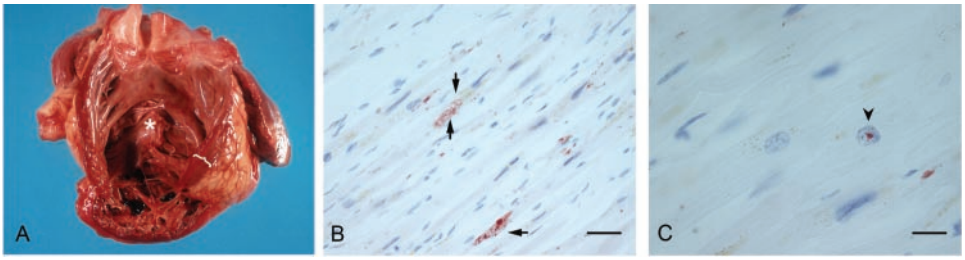

Fig. 5 Cardiac pathology in IBMPFD. (**A**) Post-mortem image of the heart from Patient II displaying left ventricular dilatation (*) and thickening of the left ventricular wall (brace). (**B** and **C**) Ubiquitin immunostaining of cardiac muscle tissue. The presence of cytoplasmic (arrows) and intranuclear (arrowhead) ubiquitin-positive inclusions may be noted. (**B** and **C**) Alkaline phosphatase anti-alkaline phosphatase staining (APAP). Bars: (**B**) 50 μm, (**C**) 15 μm.

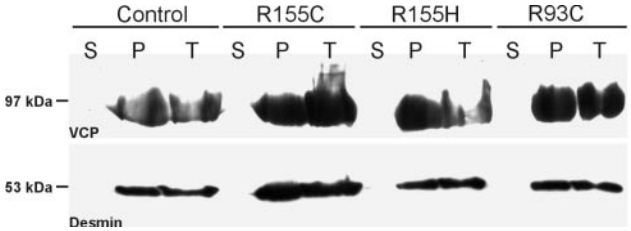

Fig. 6 VCP immunoblot analysis of normal and IBMPFD muscle. Western blotting of equal amounts of total protein extracts (T), soluble (S), and pellet fractions (P) from normal (Control) and diseased (R155C, R155H, R93C) skeletal muscle. Desmin labelling (53 kDa) was used as an internal loading control. VCP-immunoblotting detected a single band corresponding to a molecular weight of ~97 kDa in pellet and total protein fractions of all probes analysed.

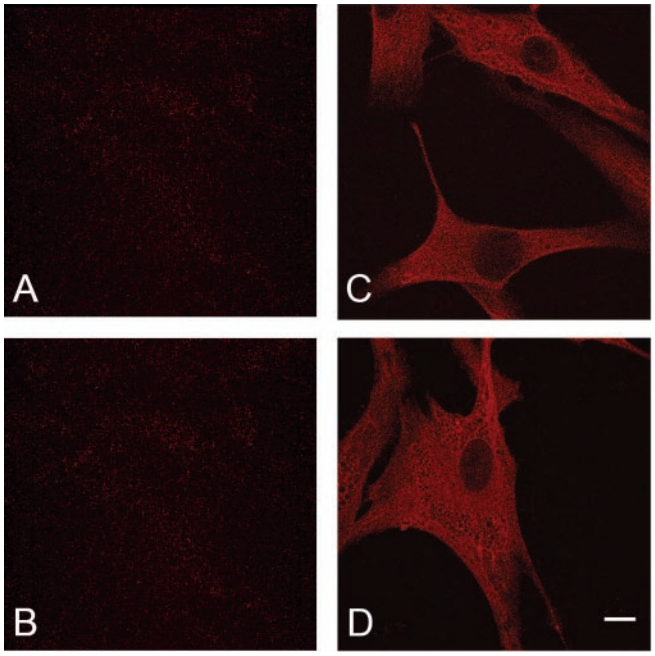

Fig. 7 Confocal immunofluorescence images of IBMPFD (**A** and **C**; R155C) and normal (**B** and **D**) primary human myoblasts. Cells were stained with an antibody directed against poly-ubiquitin (FK2). (**A** and **B**) Controls, lacking the primary antibody. It may be noted that both normal and IBMPFD myoblasts display an identical reticular FK2-staining pattern without any evidence of FK2-positive protein aggregates; bar = 20 μm.

R155C-VCP-FLAG mutant were stably expressed in C2F3 myoblasts. Transfected cells were analysed by life cell imaging and indirect immunofluorescence analysis after methanol or paraformaldehyde fixation. Expression of either N- or C-terminally tagged wt-VCP-constructs in HEK293 cells resulted in an intense labelling of the entire cytoplasm and, inconsistently, in a weaker nuclear signal of the GFP-fusion proteins (Fig. 8A, B, D and E; and data not shown). Mutant VCP showed the same localization as wt-VCP, with no evidence of abnormal cytoplasmic protein aggregate formation in HEK293 and C2F3 cells. Transfection of GFP alone yielded a strong uniform labelling of both the cytoplasm and the nucleus (Fig. 8C and F).

Furthermore, we performed stable transfections of HEK293 and C2F3 cells. Two months after the initial transfection, cells were analysed by life cell imaging. The localization of the three VCP mutants was indistinguishable from wt-VCP, with no evidence of protein aggregate formation (Fig. 8). Even Triton X-100 treatment before or after fixation of HEK293 cells did not unmask any protein aggregates (data not shown). Additionally, we performed indirect immunofluorescence analysis of the transfected HEK293 cells using antibodies directed against VCP, FLAG and poly-ubiquitinated proteins (FK2). Here, VCP and FLAG labelling showed a pattern analogous to N- or C-terminally GFP- or FLAG-tagged wt- and mutant-VCP constructs in living and fixed cells (data not shown). The FK2 antibody, a sensitive marker for pathological aggregates containing poly-ubiquitinated proteins, showed a diffuse cytoplasmic staining with occasional small foci displaying accentuated FK2 immunolabelling in the cytoplasm and nucleus of non-transfected (Fig. 10B) as well as transfected (wt-, R93C-, R155H-, R155C-VCP) HEK293 cells (Fig. 8).

In order to rule out effects of the GFP-tag, we retrovirally transduced C2F3 (a subclone of C2C12) myoblasts using wt-VCP-FLAG and R155C-VCP-FLAG expression constructs. Anti-FLAG- (Fig. 9A–D) and anti-VCP-staining (data not shown) revealed an intense labelling of the entire cytoplasm

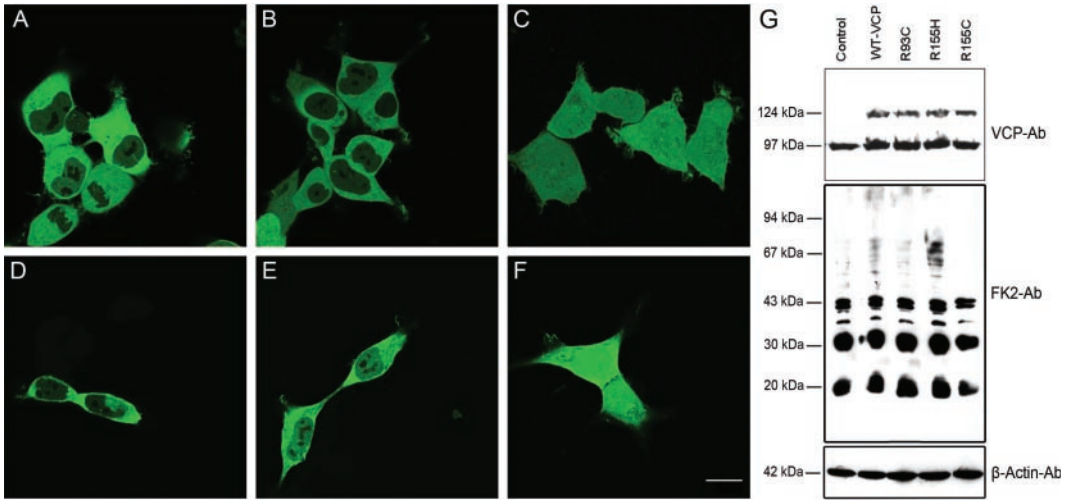

Fig. 8 Confocal images of HEK293 cells stably expressing wt- or mutant-VCP-GFP protein. (**A**–**C**) GFP signals of living cells expressing wt-VCP-GFP (**A**), R155C-VCP-GFP (**B**) and GFP as a control (**C**). (**D**–**F**) GFP signals after paraformaldehyde fixation of cells expressing wt-VCP-GFP (**D**), R155C-VCP-GFP (**E**) and GFP (**F**); bar = 20 μm. (**G**) Western blot analysis of total protein extracts from non-transfected and transfected cells as indicated. β-Actin was used as an internal loading control (lower panel). The ratio of 3:1 of endogenous versus GFP-fusion proteins (upper panel) may be noted. Poly-ubiquitin western blotting (FK2) revealed no significant differences in the pattern of immunolabelled proteins in all probes analysed (middle panel).

and, inconsistently, a weaker nuclear signal. Transduced C2F3 cells differentiated into myotubes showed the same results (Fig. 9E and F). However, neither myoblasts nor up to 6-day-old myotubes showed any evidence of protein aggregates.

For further biochemical analysis of our transfected HEK293 cells, we performed immunoblotting of total protein extracts using VCP, GFP, FLAG and FK2 antibodies. VCP immunoblotting labelled the endogenous VCP protein as well as the GFP–VCP fusion protein. The GFP and FLAG antibodies exclusively detected the respective fusion proteins (data not shown). Comparison of signal intensities indicated an endogenous VCP to wt-, R93C-, R155H and R155C–VCP fusion protein ratio of 3 : 1 (Fig. 8G). Immunoblotting after differential centrifugation of cell lysates showed that both the endogenous VCP and wt-, R93C-, R155H-, R155C–VCP fusion proteins are almost exclusively present in the soluble fraction (data not shown). In contrast to normal and IBMPFD muscle, transfections of cells with wt and mutant VCP are not associated with a detectable shift of both VCP proteins to the pellet fraction. FK2 immunoblotting revealed identical patterns of poly-ubiquitinated proteins in all samples analysed (Fig. 8G).

VCP immunoblotting after 2D gel electrophoresis of total protein extracts from wt-VCP-FLAG and R155C-VCP-FLAG transduced C2F3 myoblasts differentiated into myotubes showed an identical pattern to the one in normal and IBMPFD muscle (data not shown).

VCP response to cellular stress

Stably transfected and non-transfected HEK293 cells were treated with mitomycin C (DNA-alkylating agent), UV radiation (DNA and protein cross-linking), H_2O_2 (oxidative stress), osmotic shock, wortmannin (PI3-kinase inhibitor), *clasto*-lactacystin β-lactone (irreversible 20S proteasome inhibitor) or MG132 (reversible 26S proteasome inhibitor). Changes in the subcellular VCP-distribution of stably transfected cells were only observed in response to MG132 treatment. In C-terminally GFP-tagged wt-VCP- or R93C-, R155H-, R155C-VCP cells treatment with this reversible 26S proteasome inhibitor resulted in the formation of a single perinuclear aggregate with marked GFP signal intensity in all cells analysed (Fig. 10G and I). However, these protein aggregates showed no labelling with the FK2 antibody (Fig. 10H and J) or phalloidin (data not shown). Furthermore, ~80% of the cells additionally displayed few small foci of intranuclear protein aggregates.

Structural analysis of wild-type VCP versus R93 and R155 mutant VCP

All three VCP mutations identified in our IBMPFD patients concern evolutionarily highly conserved arginine residues in the CDC48 domain of the VCP protein (Fig. 11A). We introduced the R93C, R155H and R155C mutations into a human VCP protein model derived from the murine VCP crystal structure (*see* Material and methods). Our analysis indicates that R93 and R155 are surface-accessible residues located in the centre of cavities that may enable ligand binding (Fig. 11B). Both R93 and R155 are also surface-accessible in the hexameric state of VCP (data not shown). While the cleft around R155 is larger and predominantly negatively charged (Fig. 11C), the cavity around R93 appears smaller and rather positively charged (Fig. 11D). The particular shape and charge distribution within the clefts

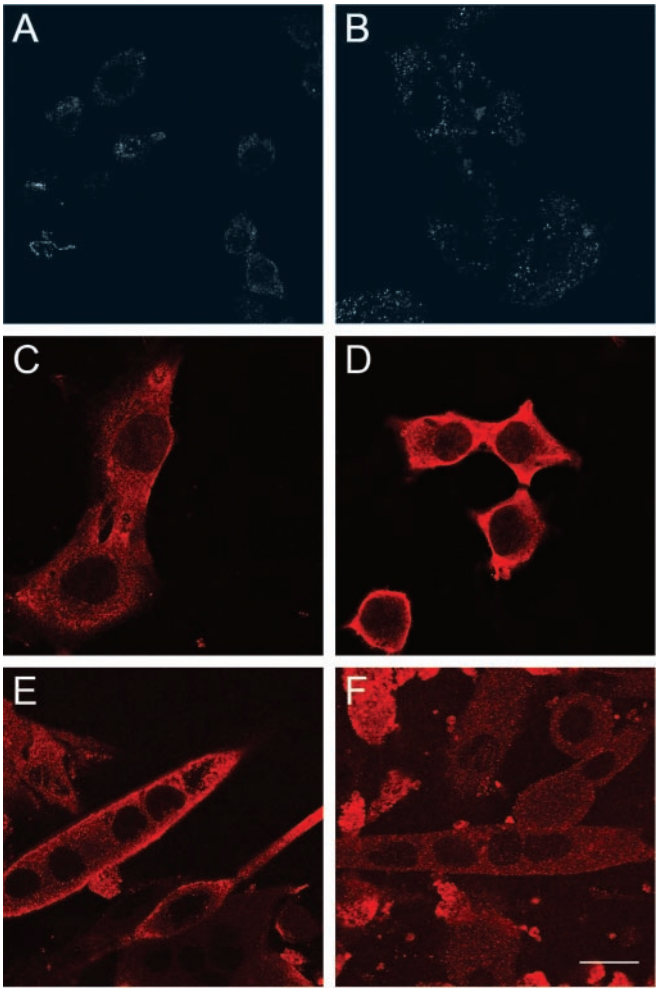

Fig. 9 Confocal immunofluorescence images of retrovirally transduced C2F3 myoblasts and myotubes expressing wt- or mutant-VCP-FLAG protein. Cells were stained with an antibody directed against the FLAG-epitope. Controls, immunofluorescence images of untransduced cells (**A**) and of wt-VCP-FLAG expressing myoblasts lacking the primary antibody (**B**). Distribution of wt-VCP-FLAG in myoblasts (**C**) and differentiated myotubes (**E**). Localization of R155C-VCP-FLAG in myoblasts (**D**) and differentiated myotubes (**F**); bar = 20 μm.

around R93 and R155 indicate that these may be putative ligand-binding sites.

Further analysis revealed that R93 maintains interactions with amino acid residues E194 and R65, as well as with the backbone carbonyl group of N90. These interactions are all within the cleft around R93. The R93C mutation leads to a loss of these contacts due to the shorter side chain of cystein. In contrast, R155 interacts with amino acid residue N387 residing in the D1-domain, which binds and hydrolyses ATP. The N- and D1-domains are spatially separated and form only three direct contacts, R155-N387, R89-E261 and E30-K217. The mutations R155C and R155H lack the interaction with N387 owing to the shorter amino acid side chains and thus may alter the relative orientation of the N- and D1-domains of VCP.

Protein-binding studies

We studied the binding of recombinant VCP to various ERAD-VCP-co-factors and other known ligands. Our GST pull-down assays demonstrated that wt-VCP as well as all three VCP mutants showed identical binding to Ufd1- (Fig. 12), Npl4- and ataxin-3 (data not shown). Furthermore, we tested whether purified wild-type and mutant VCP lacking the GST-tag can form insoluble aggregates *in vitro*. The formation of SDS-insoluble VCP aggregates was monitored by the filter retardation assay (Wanker *et al.*, 1999). These experiments showed that neither mutant VCP nor wild-type VCP formed SDS-insoluble aggregates *in vitro* (data not shown).

Virtual screening of ligand databases

We used the automated docking programme LIDAEUS to screen a small-molecule database for potential ligands for the two putative R93 and R155 ligand-binding pockets. The virtual screening approach considering docking and chemical interaction indicated that ADP/ATP are unlikely binding partners for the R155 site, but identified a steroid (16α-hydroxypregnenolone; Sigma H8252; SPH1-005-061) as well as a hexose-like compound (*N*-acetyl-α-D-glucosamine-1-phosphate disodium salt; Sigma A2142; SPH1-000-376) as ligands with significantly higher binding scores than all other target screened compounds (Fig. 13A). Although the R155 pocket is not a typical steroid binding pocket (Tanenbaum *et al.*, 1998; Williams and Sigler, 1998; Bledsoe *et al.*, 2002; Li *et al.*, 2005), some of the VCP:SPH1-005-061 interacting residues are analogous to the amino acid–steroid contacts made by the steroid receptors.

For the R93 pocket screening yielded a number of putative target molecules. The highest scoring compounds were the cyclic sugars (α-D-glucose-1-phosphate disodium salt; Sigma G7000; SPH1-004-510 and α-D-galacturonic acid-1-phosphate lithium salt; Sigma G4884; SPH1-004-402) (Fig. 13B).

Discussion

VCP mutation analysis in our three German IBMPFD patients revealed a novel heterozygous R93C mutation in Patient I and R155C and R155H mutations in Patients II and III, respectively. Our histopathological analysis revealed a broad spectrum of pathological changes in muscle reflecting different stages of disease progression in our three IBMPFD patients. Immunostaining using VCP antibodies demonstrated the presence of VCP-positive cytoplasmic aggregates, a phenomenon described previously (Watts *et al.*, 2004). Our analysis demonstrated that these VCP-positive aggregates also display positive ubiquitin staining. As a further novel finding we demonstrated the presence of VCP- and ubiquitin-positive nuclear inclusions in muscle. This aspect mirrors the brain pathology in IBMPFD, which is characterized by the presence of VCP- and ubiquitin-positive nuclear inclusions in neurons (Schröder *et al.*, 2005).

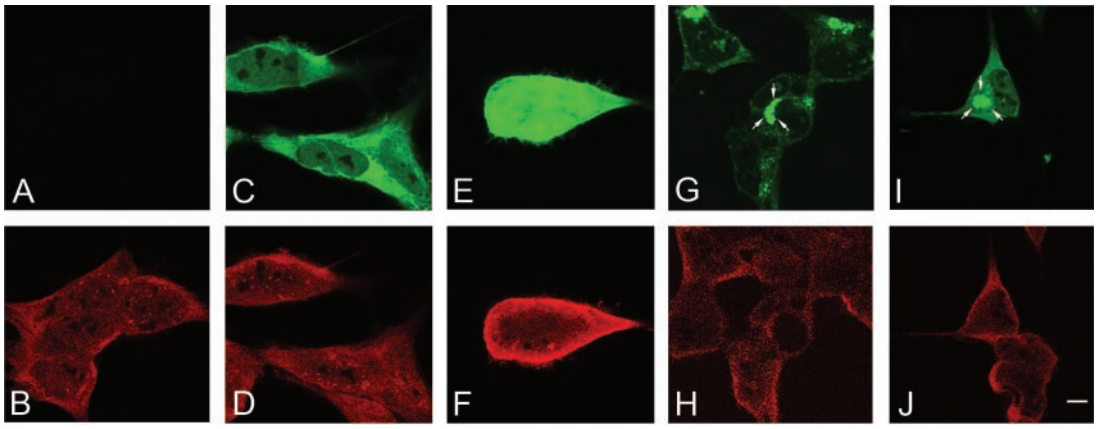

Fig. 10 Confocal immunofluorescence images of HEK293 cells stably expressing wt- or mutant-VCP-GFP non-treated (**A**–**D**) or treated by MG132 (**E**–**J**) (green = GFP; red = poly-ubiquitin, FK2 antibody). (**A**) Wt-VCP-GFP transfected HEK293 cells stained with secondary antibody only. (**B**) Untransfected HEK293 cells stained with the FK2 antibody. (**C** and **D**) Untreated cells expressing wt-VCP-GFP, and treated HEK293 cells expressing GFP only (**E** and **F**) do not display any protein aggregation. The use of MG132 resulted in the formation of marked perinuclear VCP-positive aggregates (arrows) in both wt-VCP-GFP (**G** and **H**) and R155C-VCP-GFP (**I** and **J**) cells. It may be noted that the VCP-positive aggregates lack FK2-staining; bar = 40 μm.

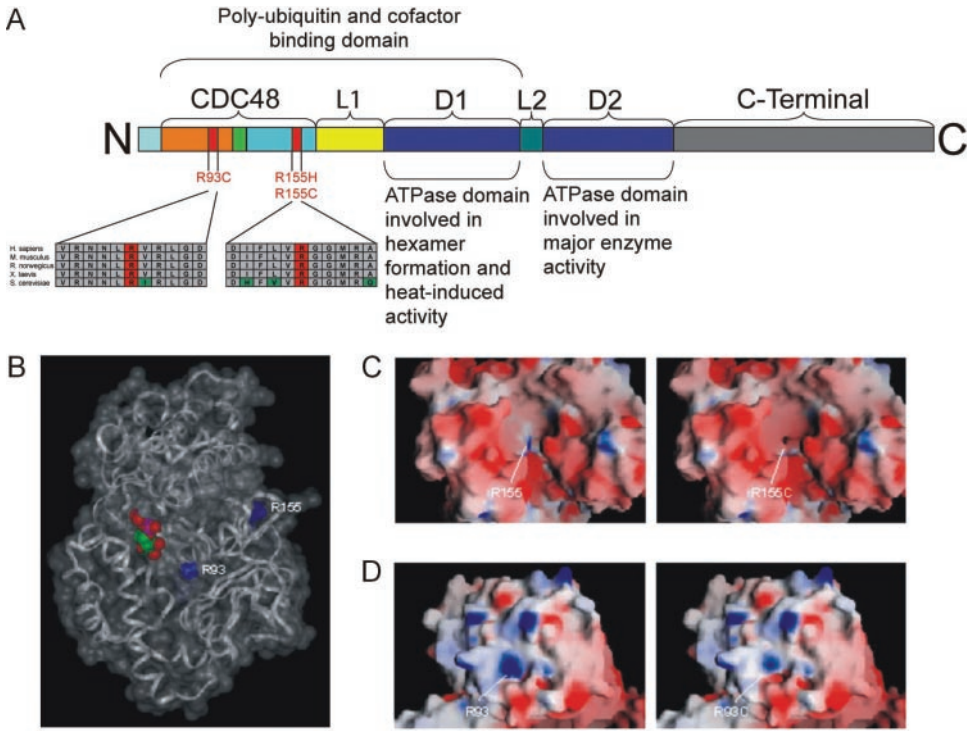

Fig. 11 (**A**) Domain structure of VCP protein: CDC48 domain composed of double ψ barrel (amino acids 25–106, orange) and the four-stranded β barrel (amino acids 112–186, cyan), connected by a short linker region (amino acids 107–111, green). The CDC48 domain connects the D1-AAA-ATPase domain (amino acids 208–459, blue) by a linker region (amino acids 187–208, yellow). Linker region L2 (dark grey), second AAA-ATPase domain (amino acids 481–761, D2, dark blue) and C-domain (amino acids 762–806, grey) are indicated. Mutations detected in our three German IBMPFD patients affect evolutionarily highly conserved arginine residues in codon 93 and codon 155 of the CDC48 domain. (**B**) Transparent Connolly surface with ribbon backbone of the human VCP model. The bound ADP in the D1-nucleotide-binding site is shown as Corey, Pauling, Koltun colouring scheme. The locations of the clefts around R93 and R155 are indicated by blue colouring of the surface of the two arginine residues; prepared with InsightII. (**C** and **D**) GRASP (Nicholls *et al*., 1993) surface representations coloured by electrostatic surface potential (red: negative, blue: positive). Shown are the clefts around R155 (**C**), as well as R93 (**D**). Wt R155 and R93 are represented on the left, while mutant R155C and R93C are shown on the right.

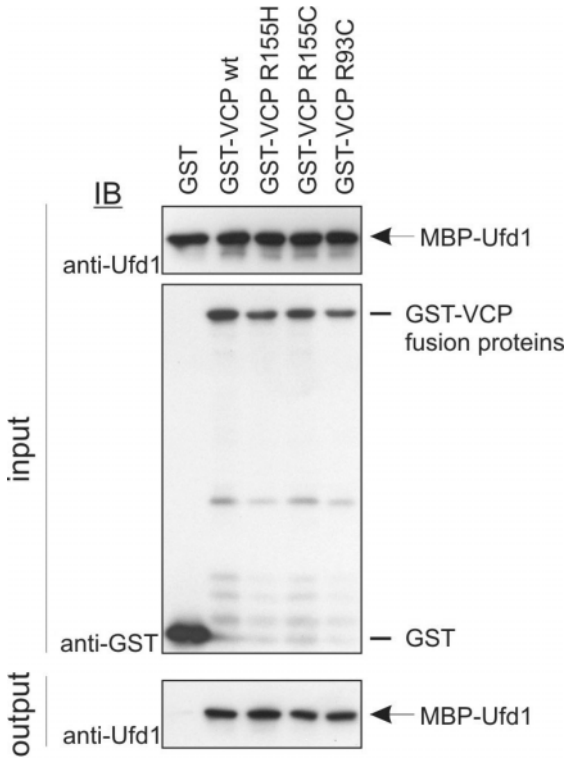

Fig. 12 GST pull-down experiments with purified MBP-Ufd1. GST–VCP fusion proteins were bound to glutathione agarose beads and incubated with MBP-Ufd1. After extensive washing of the beads, bound protein was detected by immunoblotting using an anti-Ufd1 antibody (bottom panel). Ten per cent of the input binding mixture was subjected to immunoblot analysis with anti-Ufd1 (top panel) and anti-GST antibody (middle panel).

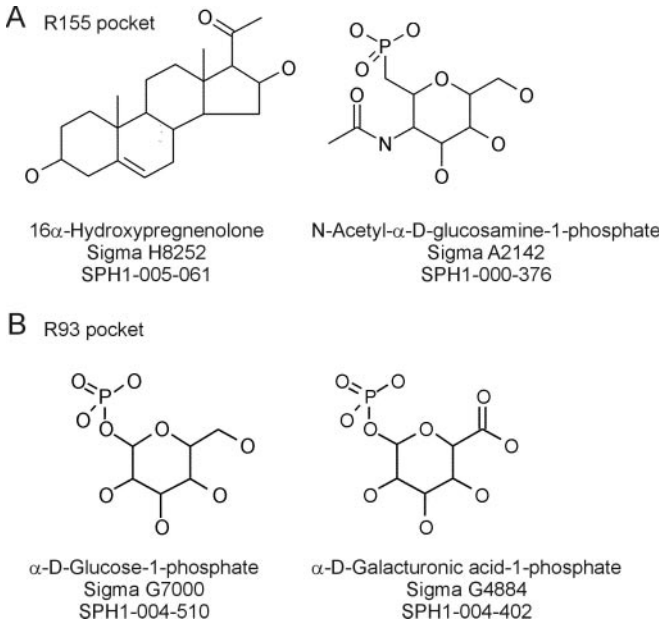

Fig. 13 Selected putative lead compounds suggested by LIDAEUS and confirmed by visual inspection of the docked ligands in the R155 (**A**) and R93 (**B**) pocket.

Our ultrastructural analysis demonstrated that both the cytoplasmic and the nuclear inclusions in IBMPFD muscle were composed of haphazardly arranged filaments.

In analogy to the aberrant desmin immunofluorescence staining, our ultrastructural studies revealed the presence of desmin-positive granulofilamentous material, the characteristic ultrastructural hallmark of primary desminopathies and myofibrillar myopathies (Schröder *et al.*, 2003; Selcen *et al.*, 2004; Bär *et al.* 2005). This finding indicates that, at least in advanced degenerative stages of IBMPFD, VCP mutations induce secondary alterations of the extrasarcomeric desmin cytoskeleton.

The post-mortem analysis of Patient II revealed a novel clinical aspect in IBMPFD. VCP mutations not only affect skeletal muscle but may also lead to a dilatative cardiomyopathy characterized by ubiquitin-positive cytoplasmic aggregates and nuclear inclusions. This novel aspect clearly warrants appropriate clinical awareness and repeated cardiological work-up in IBMPFD patients.

Our immunoblotting analyses revealed no significant differences in the total amount, subcellular distribution and post-translational modifications of VCP protein between normal and diseased muscle. In contrast to IBMPFD muscle, where endogenous VCP is solely present in the insoluble fraction, western blot analysis of transfected cells (wt and mutant VCP) demonstrated that endogenous and transfected VCP is predominately present in the soluble protein fraction.

In contrast to IBMPFD muscle our transient and stable transfection experiments using mutant and wt VCP did not lead to cytoplasmic or nuclear protein aggregate formation. In line with previous studies (Meriin *et al.* 1998), aggresome formation could be elicited using the proteasome inhibitor MG132 in HEK293 cells, but no apparent differences in the extent or subcellular localization of aggresomes were noted in cells either transfected with wt or mutant VCP. All other stress experiments as well as differentiation of C2F3 myoblasts into myotubes did not provide any evidence suggesting abnormal protein aggregate formation.

These findings are in contrast to the recently published study by Weihl *et al.* (2006), who described large perinuclear aggregates in up to 33% of cells transfected with R155H-VCP-GFP and R95G-VCP-GFP and in 7% of cells transfected with wt-VCP-GFP. These aggregates were reported to contain poly-ubiquitinated proteins; a subgroup also mutated VCP protein. A potential cause for aggregates in such transient transfection experiments may be strong overexpression of the transfected gene. This is strongly supported by the following reasons. (i) A previous study by Ye *et al.* (2004) demonstrated strikingly similar perinuclear aggregates in double transient transfection studies using His-wt-VCP and Myc-wt-VIMP, a membrane protein that recruits the VCP-ATPase. (ii) In our immunoblot-controlled stable transfections a ratio of 1:3 of mutant VCP to wt VCP did not lead to protein aggregate formation. (iii) In primary

human myoblasts derived from IBMPFD skeletal muscle, which most closely represent the physiological situation with one wt and one mutated VCP allele, no abnormal protein aggregation was detected by VCP and FK2 immunostaining. (iv) In the vast majority of IBMPFD patients, it takes at least 40–50 years until the disease manifests and protein aggregates are exclusively found in post-mitotic cells (neurons, striated muscle cells). Taken together, these findings strongly implicate that these cell culture models are of very limited value in studying IBMPFD-associated protein aggregate formation.

VCP and its co-factors Ufd1 and Npl4 are part of the ERAD pathway, which has a crucial role in removing misfolded proteins from the endoplasmic reticulum (Lederkremer and Glickman, 2005). In GST pull-down experiments no detectable changes in the binding of recombinant Ufd1 and Npl4 to wt and mutant VCP could be observed. Moreover, binding analysis of wt and mutant VCP to Udf1, Npl4 and ataxin-3, well-established VCP-ligands, showed identical results. Furthermore, in a previous study, the ATPase-activity of purified R155H-VCP was similar to the one reported for wt-VCP (Weihl *et al.*, 2006). These results imply that the various VCP mutants analysed so far are not associated with gross alterations in VCP binding to known co-factors and its intrinsic ATPase enzyme activity. This favours the hypothesis that IBMPFD pathology is due to a toxic gain of VCP function.

All three VCP mutations identified in our IBMPFD patients affect evolutionarily highly conserved arginine residues in the CDC48 domain of the VCP protein. R93 and R155 are both surface-accessible residues (in monomeric and hexameric VCP) located in the centre of cavities that may enable ligand binding. R155 interacts with amino acid residue N387 residing in the D1-domain, which binds and hydrolyses ATP. The mutations R155C and R155H lack the interaction with N387 and thus may alter the relative orientation of the N- and D1-domains of VCP. DeLaBarre and Brünger (2003) proposed a model where the mobile state of the N-domain is triggered by release of a latch provided by the D1α-domain. Three pairs of residues can be identified that could act as latch. Importantly, one of these pairs is R155-N387. A VCP mutant with an impaired ability to lock the N-domain is very likely to have lost its regulatory properties. R93 maintains interactions with amino acid residues E194 and R65, as well as with the backbone carbonyl group of N90. The R93C mutation leads to a loss of these contacts due to the shorter side chain of cystein.

Our screening of a small-molecule database identified a steroid (16α-hydroxypregnenolone) as well as a hexose-like compound (*N*-acetyl-α-D-glucosamine-1-phosphate) and the cyclic sugar compounds α-D-glucose-1-phosphate and α-D-galacturonic acid-1-phosphate for the R155 and R93 binding pockets, respectively. The appearance of sugar-like compounds for the R93 site establishes a link to the reported interactions between $SCF^{(Fbs1,2)}$, a cytosolic ubiquitinase for glycoproteins and VCP (Yoshida *et al.*, 2005). Here, it is tempting to speculate that VCP mutations interfere with the binding to carbohydrates from misfolded glycoproteins in the endoplasmic reticulum and cytosol (Spiro, 2002).

Acknowledgements

We thank Wolfram Kress (Institute of Human Genetics, University of Würzburg, Germany), for desmin and αβ-crystalline mutation analysis in Patient II. Furthermore, the excellent technical assistance of Ms K. Kappes-Horn, Ms M. Stepien-Mering, Ms S. Plassmann, Ms M. Schmuck and Ms E. Schmidtmeyer is gratefully acknowledged. R. Schröder, H. Lochmüller and B. Schoser are members of the German network on muscular dystrophies (*MD-NET*; 01GM0302) funded by the German ministry of education and research (BMBF, Bonn, Germany). Human myoblast cultures were obtained from the Muscle Tissue Culture Collection (Friedrich-Baur-Institute, Munich, Germany), part of the *MD-NET* (service structure S1), partner of EuroBioBank (www.eurobiobank.org). We thank P. Taylor and M. Walkinshaw (Edinburgh) for access to the virtual screening software.

References

Ardley HC, Scott GB, Rose SA, Tan NG, Markham AF, Robinson PA. Inhibition of proteasomal activity causes inclusion formation in neuronal and non-neuronal cells overexpressing Parkin. Mol Biol Cell 2003; 14: 4541–56.

Bär H, Fischer D, Goudeau B, Kley RA, Clemen CS, Vicart P, et al. Pathogenic effects of a novel heterozygous R350P desmin mutation on the assembly of desmin intermediate filaments in vivo and in vitro. Hum Mol Genet 2005; 14: 1251–60.

Bledsoe RK, Montana VG, Stanley TB, Delves CJ, Apolito CJ, McKee DD, et al. Crystal structure of the glucocorticoid receptor ligand binding domain reveals a novel mode of receptor dimerization and coactivator recognition. Cell 2002; 110: 93–105.

Boeddrich A, Gaumer S, Haacke A, Tzvetkov N, Albrecht M, Evert BO, et al. An arginine/lysine-rich motif is crucial for VCP/p97-mediated modulation of ataxin-3 fibrillogenesis. EMBO J 2006; 25: 1547–58.

Clemen CS, Hofmann A, Zamparelli C, Noegel AA. Expression and localisation of annexin VII (synexin) isoforms in differentiating myoblasts. J Muscle Res Cell Motil 1999; 20: 669–79.

Clemen CS, Fischer D, Roth U, Simon S, Vicart P, Kato K, et al. Hsp27-2D-gel electrophoresis is a diagnostic tool to differentiate primary desminopathies from myofibrillar myopathies. FEBS Lett 2005; 579: 3777–82.

D'Alessandro M, Russell D, Morley SM, Davies AM, Lane EB. Keratin mutations of epidermolysis bullosa simplex alter the kinetics of stress response to osmotic shock. J Cell Sci 2002; 115: 4341–51.

DeLaBarre B, Brunger AT. Complete structure of p97/valosin-containing protein reveals communication between nucleotide domains. Nat Struct Biol 2003; 10: 856–63.

Dreveny I, Kondo H, Uchiyama K, Shaw A, Zhang X, Freemont PS. Structural basis of the interaction between the AAA ATPase p97/VCP and its adaptor protein p47. EMBO J 2004; 23: 1030–9.

Fischer D, Walter MC, Kesper K, Petersen JA, Aurino S, Nigro V, et al. Diagnostic value of muscle MRI in differentiating LGMD2I from other LGMDs. J Neurol 2005; 252: 538–47.

Haubenberger D, Bittner RE, Rauch-Shorny S, Zimprich F, Mannhalter C, Wagner L, et al. Inclusion body myopathy and Paget disease is linked to a novel mutation in the VCP gene. Neurology 2005; 65: 1304–5.

Hetzer M, Meyer HH, Walther TC, Bilbao-Cortes D, Warren G, Mattaj IW. Distinct AAA-ATPase p97 complexes function in discrete steps of nuclear assembly. Nat Cell Biol 2001; 3: 1086–91.

Hirabayashi M, Inoue K, Tanaka K, Nakadate K, Ohsawa Y, Kamei Y, et al. VCP/p97 in abnormal protein aggregates, cytoplasmic vacuoles, and cell death, phenotypes relevant to neurodegeneration. Cell Death Differ 2001; 8: 977–84.

Jones TA, Zou JY, Cowan SW, Kjeldgaard. Improved methods for building protein models in electron density maps and the location of errors in these models. Acta Crystallogr A 1991; 47: 110–9.

Kitami MI, Kitami T, Nagahama M, Tagaya M, Hori S, Kakizuka A, et al. Dominant-negative effect of mutant valosin-containing protein in aggresome formation. FEBS Lett 2006; 580: 474–8.

Kondo H, Rabouille C, Newman R, Levine TP, Pappin D, Freemont P, et al. p47 is a cofactor for p97-mediated membrane fusion. Nature 1997; 388: 75–8.

Laskowski R, MacArthur M, Moss D, Thornton J. PROCHECK: a program to check the stereochemical quality of protein structures. J Appl Cryst 1993; 26: 283–91.

Lederkremer GZ, Glickman MH. A window of opportunity: timing protein degradation by trimming of sugars and ubiquitins. Trends Biochem Sci 2005; 30: 297–303.

Li Y, Suino K, Daugherty J, Xu HE. Structural and biochemical mechanisms for the specificity of hormone binding and coactivator assembly by mineralocorticoid receptor. Mol Cell 2005; 19: 367–80.

Lilley BN, Ploegh HL. Multiprotein complexes that link dislocation, ubiquitination and extraction of misfolded proteins from the endoplasmic reticulum membrane. Proc Natl Acad Sci USA 2005; 102: 14296–301.

Meriin AB, Gabai VL, Yaglom J, Shifrin VI, Sherman MY. Proteasome inhibitors activate stress kinases and induce Hsp72. Diverse effects on apoptosis. J Biol Chem 1998; 273: 6373–9.

Meyer HH, Shorter JG, Seemann J, Pappin D, Warren G. A complex of mammalian ufd1 and npl4 links the AAA-ATPase, p97, to ubiquitin and nuclear transport pathways. EMBO J 2000; 19: 2181–92.

Mizuno Y, Hori S, Kakizuka A, Okamoto K. Vacuole-creating protein in neurodegenerative diseases in humans. Neurosci Lett 2003; 343: 77–80.

Nan L, Wu Y, Bardag-Gorce F, Li J, French BA, Wilson LT, et al. RNA interference of VCP/p97 increases Mallory body formation. Exp Mol Pathol 2005; 78: 1–9.

Nicholls A, Bharadwaj R, Honig B. GRASP: graphical representation and analysis of surface properties. Biophys J 1993; 64: A166.

Noegel AA, Blau-Wasser R, Sultana H, Muller R, Israel L, Schleicher M, et al. The cyclase-associated protein CAP as regulator of cell polarity and cAMP signaling in Dictyostelium. Mol Biol Cell 2004; 15: 934–45.

Rabinovich E, Kerem A, Frohlich KU, Diamant N, Bar-Nun S. AAA-ATPase p97/Cdc48p, a cytosolic chaperone required for endoplasmic reticulum-associated protein degradation. Mol Cell Biol 2002; 22: 626–34.

Rabouille C, Kondo H, Newman R, Hui N, Freemont P, Warren G. Syntaxin 5 is a common component of the NSF- and p97-mediated reassembly pathways of Golgi cisternae from mitotic Golgi fragments in vitro. Cell 1998; 92: 603–10.

Rarey M, Wefing S, Lengauer T. Placement of medium-sized molecular fragments into active sites of proteins. J Comput Aided Mol Des 1996; 10: 41–54.

Scherzinger E, Lurz R, Turmaine M, Mangiarini L, Hollenbach B, Hasenbank R, et al. Huntingtin-encoded polyglutamine expansions form amyloid-like protein aggregates in vitro and in vivo. Cell 1997; 90: 549–58.

Schröder R, Kunz WS, Rouan F, Pfendner E, Tolksdorf K, Kappes-Horn K, et al. Disorganization of the desmin cytoskeleton and mitochondrial dysfunction in plectin-related epidermolysis bullosa simplex with muscular dystrophy. J Neuropathol Exp Neurol 2002; 61: 520–30.

Schröder R, Goudeau B, Simon MC, Fischer D, Eggermann T, Clemen CS, et al. On noxious desmin: functional effects of a novel heterozygous desmin insertion mutation on the extrasarcomeric desmin cytoskeleton and mitochondria. Hum Mol Genet 2003; 12: 657–69.

Schröder R, Watts GD, Mehta SG, Evert BO, Broich P, Fliessbach K, et al. Mutant valosin-containing protein causes a novel type of frontotemporal dementia. Ann Neurol 2005; 57: 457–61.

Selcen D, Ohno K, Engel AG. Myofibrillar myopathy: clinical, morphological and genetic studies in 63 patients. Brain 2004; 127: 439–51.

Spiro RG. Protein glycosylation: nature, distribution, enzymatic formation, and disease implications of glycopeptide bonds. Glycobiology 2002; 12: 43R–56R.

Steinhilb ML, Turner RS, Gaut JR. The protease inhibitor, MG132, blocks maturation of the amyloid precursor protein Swedish mutant preventing cleavage by beta-Secretase. J Biol Chem 2001; 276: 4476–84.

Tait D, Riccio M, Sittler A, Scherzinger E, Santi S, Ognibene A, et al. Ataxin-3 is transported into the nucleus and associates with the nuclear matrix. Hum Mol Genet 1998; 7: 991–7.

Tanenbaum DM, Wang Y, Williams SP, Sigler PB. Crystallographic comparison of the estrogen and progesterone receptor's ligand binding domains. Proc Natl Acad Sci USA 1998; 95: 5998–6003.

Vicart P, Caron A, Guicheney P, Li Z, Prevost MC, Faure A, et al. A missense mutation in the alphaB-crystallin chaperone gene causes a desmin-related myopathy. Nat Genet 1998; 20: 92–5.

Waelter S, Boeddrich A, Lurz R, Scherzinger E, Lueder G, Lehrach H, et al. Accumulation of mutant Huntingtin fragments in aggresome-like inclusion bodies as a result of insufficient protein degradation. Mol Biol Cell 2001; 12: 1393–407.

Wallace AC, Laskowski RA, Thornton JM. LIGPLOT: a program to generate schematic diagrams of protein-ligand interactions. Protein Eng 1995; 8: 127–34.

Wanker EE, Scherzinger E, Heiser V, Sittler A, Eickhoff H, Lehrach H. Membrane filter assay for detection of amyloid-like polyglutamine-containing protein aggregates. Methods Enzymol 1999; 309: 375–86.

Watts GD, Wymer J, Kovach MJ, Mehta SG, Mumm S, Darvish D, et al. Inclusion body myopathy associated with Paget disease of bone and frontotemporal dementia is caused by mutant valosin-containing protein. Nat Genet 2004; 36: 377–81.

Weihl CC, Dalal S, Pestronk A, Hanson PI. Inclusion body myopathy-associated mutations in p97/VCP impair endoplasmic reticulum-associated degradation. Hum Mol Genet 2006; 15: 189–99.

Westfall MD, Joyner AS, Barbieri CE, Livingstone M, Pietenpol JA. Ultraviolet radiation induces phosphorylation and ubiquitin-mediated degradation of DeltaNp63alpha. Cell Cycle 2005; 4: 710–6.

Williams SP, Sigler PB. Atomic structure of progesterone complexed with its receptor. Nature 1998; 393: 392–6.

Wu SY, McNae I, Kontopidis G, McClue SJ, McInnes C, Stewart KJ, et al. Discovery of a novel family of CDK inhibitors with the program LIDAEUS: structural basis for ligand-induced disordering of the activation loop. Structure 2003; 11: 399–410.

Ye Y, Meyer HH, Rapoport TA. The AAA ATPase Cdc48/p97 and its partners transport proteins from the ER into the cytosol. Nature 2001; 414: 652–6.

Ye Y, Shibata Y, Yun C, Ron D, Rapoport TA. A membrane protein complex mediates retro-translocation from the ER lumen into the cytosol. Nature 2004; 429: 841–7.

Yoshida Y, Adachi E, Fukiya K, Iwai K, Tanaka K. Glycoprotein-specific ubiquitin ligases recognize N-glycans in unfolded substrates. EMBO Rep 2005; 6: 239–44.